A Practical Method to Evaluate Failure Envelopes of Shallow Foundations Considering Soil Strain Softening and Rate Effects

Zhong Xiao[a, *], Yinghui Tian[a, b] and Susan Gourvenec[b]

Published in *Applied Ocean Research,* 59: 395-407. http://dx.doi.org/10.1016/j.apor.2016.06.015

Zhong XIAO (corresponding author)
Associate Professor
[a]State Key Laboratory of Hydraulic Engineering Simulation and Safety
Tianjin University
92 Weijin Road, Nankai District
Tianjin, 300072
China
Visiting scholar at Centre for Offshore Foundation Systems, University of Western Australia
Mobile phone: +86 13682033546
Email: tjuzhongxiao@tju.edu.cn

Yinghui TIAN
[a]State Key Laboratory of Hydraulic Engineering Simulation and Safety
Tianjin University
92 Weijin Road, Nankai District
Tianjin, 300072
China

Senior Research Fellow
[b]Centre for Offshore Foundation Systems, a node of the ARC Centre of Excellence for Geotechnical Science and Engineering
University of Western Australia
35 Stirling Highway, Crawley
Perth, WA 6009
Australia
Tel: +61 8 6488 7076
Email: yinghui.tian@uwa.edu.au

Susan GOURVENEC
Professor
[b]Centre for Offshore Foundation Systems, a node of the ARC Centre of Excellence for Geotechnical Science and Engineering
University of Western Australia
Tel: +61 8 6488 3094
Email: susan.gourvenec@uwa.edu.au

Submitted as original paper
No. of words: 6300 (excluding notation list, abstract and references)
No. of figures: 21

A Practical Method to Evaluate Failure Envelopes of Shallow Foundations Considering Soil Strain Softening and Rate Effects

Zhong Xiao[a, *], Yinghui Tian[a, b] and Susan Gourvenec[b]

Abstract

This paper presents a practical method to evaluate the development of failure envelopes of coastal and offshore shallow foundations after the action of multi-directional cyclic loading considering soil degradation. This is realised by implementing a soil strain softening and rate model into a finite element package and using a combined approach of load controlled geometrically nonlinear finite element analysis and displacement controlled small strain finite element analysis. The gradual evolution of soil strain softening and rate effects are monitored and utilised to update the shear strength during the analysis under multi-directional cyclic loading. The failure envelope is then investigated based on the updated shear strength field of the soil. After introducing the approach and demonstrating with an example, a systematic study is presented to explore the effects of soil strain softening and rate parameters, soil stiffness index and period of cyclic loading on load carrying capacity of coastal and offshore shallow foundations. The results show that soil degradation should be taken into account in design of coastal and offshore shallow foundations because it is detrimental to the capacity of shallow foundations. Results of the parametric analyses have shown that soil sensitivity, relative ductility and the stiffness index have more influence on capacity of shallow foundations subjected to undrained cyclic preloading than strain rate parameter and the period of cyclic loading.

Keywords: shallow foundation; failure envelope; soil degradation; undrained cyclic preloading; strain softening effect; strain rate effect

Notation list

B	Foundation width
E	Young's modulus
H	Horizontal load
H_{ult}	Pure horizontal capacity
$H_{ult,intact}$	Pure horizontal capacity on intact soil
M	Moment
M_{ult}	Pure moment capacity
$M_{ult,intact}$	Pure moment capacity on intact soil
N	The cycle number of cyclic loading
N_H	Horizontal capacity factor, = H_{ult}/Bs_{u0}
$N_{H,intact}$	Horizontal capacity factor on intact soil, = $H_{ult,intact}/Bs_{u0}$
N_M	Moment capacity factor, = M_{ult}/B^2s_{u0}
$N_{M,intact}$	Moment capacity factor on intact soil, = $M_{ult,intact}/B^2s_{u0}$
N_V	Vertical capacity factor, = V_{ult}/Bs_{u0}
$N_{V,intact}$	Vertical capacity factor on intact soil, = $V_{ult,intact}/Bs_{u0}$
S_t	Soil sensitivity
s_u	Undrained shear strength
s_{u0}	Intact undrained shear strength
T	Period of cyclic loading
u	Horizontal displacement
V	Vertical load
V_{ult}	Pure vertical capacity
$V_{ult,intact}$	Pure vertical capacity on intact soil
W'	Submerged self-weight of the foundation and superstructure

98	w	Vertical displacement
99	α_V, α_H, α_M	Vertical, horizontal and moment capacity reduction factors
100	β_s, β_r	Soil strain softening and rate factors
101	γ_c	Cyclic shear strain
102	$\dot{\gamma}_{max}$	Current maximum shear strain rate
103	$\dot{\gamma}_{ref}$	Reference shear strain rate
104	Δt	Time increment
105	ε_{p1}, ε_{p3}	Major and minor principal plastic strains
106	ε_1, ε_3	Major and minor principal total strains
107	δ_{rem}	Reciprocal of soil sensitivity, $=1/S_t$
108	θ	Rotation angle
109	μ	Rate of undrained shear strength increase per decade
110	ξ	Current accumulated absolute plastic shear strain
111	ξ_{95}	Soil relative ductility (Value of ξ for the soil undrained shear
112		strength to achieve 95% remoulding)
113		

1. Introduction

Coastal and offshore shallow foundations are subjected to a combination of vertical load (V), horizontal load (H) and moment (M). The common convention of loads (V, H and M) and the corresponding displacements (w, u and θ) are as illustrated in Fig. 1. The failure envelope approach is now well established to address shallow foundation capacity under combined loading. This method for geotechnical applications can be tracked down to Roscoe and Schofield [1] and has been increasingly used to evaluate the multi-directional capacity of offshore foundations. The majority of existing studies consider undrained soil response and rely on an initial, constant value of undrained shear strength over the period of loading [2-6]. Some studies have considered the effect of monotonic vertical preloading on the undrained shear strength distribution in the supporting soil and the resulting gains in consolidated, undrained combined load capacity [7, 8]. These latter studies are relevant for field conditions in which excess pore pressures generated during vertical preloading are able to dissipate prior to the combined loading event. For example, for subsea foundations that form part of a pipeline network, as a significant time lag is encountered between lay (or installation) and operation of the attached pipelines that impose the combined loads.

This study considers coastal and offshore shallow foundation capacity when excess pore pressures, due to multi-directional loading, do not have the opportunity to dissipate prior to a peak combined loading event. These conditions are particularly relevant to coastal breakwaters and offshore fixed bottom platforms, which are subjected not only to a static load of dead weight but also to combined cyclic loading due to environmental forces (such as waves, winds, currents and ice in arctic regions). The undrained shear strength of clays degrades under cyclic loading [9-12]. Failure of a coastal dike was reported in Yan et al. [13], which was attributed to clay strength degradation under cyclic loading in a storm.

This paper presents a practical numerical method to evaluate the evolution of failure envelopes of coastal and offshore shallow foundations after the action of multi-directional cyclic loading. The soil

strain softening and rate model proposed by Einav and Randolph [14] was adopted and implemented into the commercial finite element package ABAQUS through the user subroutine USFLD [15]. The influence of cyclic loading on the failure envelope was investigated as a function of number of cycles of loading. Sensitivity studies were carried out to provide insights into the effects of soil strain softening and rate parameters, soil stiffness index and period of cyclic loading. The study is intended to present the methodology and to provide insights for geotechnical engineers to assess the development of failure envelopes for coastal and offshore shallow foundations due to cyclic loading.

2. Strain softening and rate effect model

Among many available soil degradation models [16-19], the one proposed by Einav and Randolph [14] considers both the effects of strain softening (reducing the undrained shear strength) and strain rate (enhancing the undrained shear strength) to update the shear strength in a total stress analysis framework. The rigorous derivation from classical soil mechanics using limit analysis theory and the verification against centrifuge model tests indicate that this model is appropriate to describe the development of undrained shear strength of offshore soft clays [20]. The Einav and Randolph model has been applied previously in the most part to monotonic loading conditions and in only one case to the interpretation of shallow foundations [20], in which the model was used to replicate centrifuge tests of monotonic vertical compression and uplift of offshore shallow foundations. Limited cases of the model to cyclic loading are reported but include the application to interpretation of cyclic T-bar tests [21] and dynamic pipe installation [22]. This strain softening and rate dependent model has not yet been applied to the systematic analysis of the capacity of shallow foundations under cyclic loading.

The premise of this model is that the undrained shear strength (s_u) is evaluated based on the current accumulated absolute plastic shear strain (ζ) and current maximum shear strain rate ($\dot{\gamma}_{max}$):

$$s_u = \beta_s \beta_r s_{u0} \quad (1)$$

$$\beta_s = \delta_{rem} + (1 - \delta_{rem}) e^{-3\xi/\xi_{95}} \quad (2)$$

$$\beta_r = 1 + \mu \log\left(\frac{\max\left(|\dot{\gamma}_{max}|, \dot{\gamma}_{ref}\right)}{\dot{\gamma}_{ref}} \right) \quad (3)$$

where β_s, β_r are the strain softening and strain rate factors, respectively. s_{u0} is the intact undrained shear strength. δ_{rem} indicates the ratio between the fully remoulded and the initial undrained shear strength s_{u0}, and is equal to the reciprocal of the soil sensitivity (S_t). ξ_{95} indicates the relative ductility of the saturated clay, and is equal to the value of ξ for the soil undrained shear strength to achieve 95% remoulding. e is the natural exponent. μ indicates the rate of undrained shear strength increase per decade. $\dot{\gamma}_{ref}$ is the reference shear strain rate, and maximum shear strain rate $\dot{\gamma}_{max}$ is defined as

$$\dot{\gamma}_{max} = \frac{\Delta\varepsilon_1 - \Delta\varepsilon_3}{\Delta t} \quad (4)$$

where $\Delta\varepsilon_1$ and $\Delta\varepsilon_3$ are the major and minor principal total strain increments to occur in the duration of an increment Δt.

S_t and ξ_{95} in the range 2 ~ 6 and 10 ~ 50 respectively are recommended for marine clays [14, 23]. The strain rate parameter μ is advised to range from 0.05 to 0.2 [14, 24, 25].

3. Implementation of strain softening and rate model into finite element program

The soil response in this study was modelled as undrained considering that excess pore pressures in clay deposits do not have the opportunity to dissipate under cyclic loading in a storm. The Tresca failure criterion was adopted, which is a widespread assumption to evaluate undrained capacity for monotonic or cyclic loading boundary value problems [21, 26-28].

3.1 Key steps for implementation of constitutive model in finite element analysis

The 2 key steps to implement the combination of the Einav and Randolph model and Tresca model in the finite element program are set out below.

(1) Definition of field variable and solution-dependent state variables. A field variable is a definition of input or output data representing the value of a variable over a domain, which can be defined as an artificial field to modify certain material properties during the course of an analysis [15]. Solution-dependent state variables can be defined to evolve with the solution of an analysis, which are necessary when some information has to be remembered and used later on. One field variable and 7 solution-dependent state variables are defined in this study. The one field variable describes the evolution of shear strength (s_u). The Young's modulus (E) is directly related to s_u through a constant E/s_u ratio. The strain softening and strain rate factors (β_s, β_r) (see Eq.1) are defined as solution-dependent state variables. Meanwhile, the major and minor principal total and plastic strains (i.e. ε_1, ε_3, ε_{p1} and ε_{p3}) at the end of one increment are defined as another 4 solution-dependent state variables. Finally, the accumulated absolute plastic shear strain (ξ) is defined as the seventh solution-dependent state variable.

(2) Updating the Tresca model with field variables. The undrained shear strength (s_u) and Young's modulus (E) for the Tresca model are calculated based on field variables. This is realised by relating the Tresca model with user-defined field variable dependencies turned on in the material properties definition. At the beginning of an increment, the field variable over the whole soil domain can be obtained and the corresponding values of undrained shear strength (s_u) and Young's modulus (E) will be updated. The USDFLD subroutine defines field variables at a material point by calling the GETVRM utility routine, which extracts variables such as strain and stress [15]. The 5 solution-dependent state variables, i.e. major and minor principal total and plastic strains (ε_1, ε_3, ε_{p1} and ε_{p3}), which are provided by the GETVRM utility routine, and accumulated absolute plastic shear strain ξ at the end of one increment are stored. At the end of the current increment, the updated major and minor principal total and plastic strains (ε_1, ε_3, ε_{p1} and ε_{p3}) are again extracted using GETVRM. Then the maximum shear strain rate ($\dot{\gamma}_{max}$) at the current increment can be evaluated

according to Eq. (4) based on the stored and current major and minor principal total strains (ε_1 , ε_3 , ε_{p1} and ε_{p3}). The accumulated absolute plastic shear strain ξ is updated with the calculated strain from the current increment. Consequently, the field variable over the whole soil domain is calculated on the basis of the current accumulated absolute plastic shear strain ξ and the current maximum shear strain rate ($\dot{\gamma}_{max}$) according to Eq. (1) to Eq. (3). Soil strain softening or rate effect factors, i.e. β_s and β_r, are stored as two solution-dependent state variables. Geometrically nonlinear effects of soil elements were taken into account in this step in order to precisely evaluate the accumulated strain. It is noted that the model deformation in this study was relatively small and thus large deformation finite element analysis with remeshing was unnecessary. The geometrically nonlinear finite element analysis was selected for precision and acceptable computational time during the analysis under cyclic loading.

3.2 Validation of constitutive model

In this section, the user subroutine for the constitutive model is validated and the validity of the adopted constitutive model to capture the degradation characteristics of soft clay under cyclic loading is demonstrated and discussed.

Strain controlled 2-way symmetric cyclic loading was modelled with a period of 6s for a single element to illustrate the evolution of soil shear strength and stiffness with increasing number of cycles by using the strain softening and rate dependent model adopted in this study. The initial shearing modulus of elasticity of the soil element under cyclic horizontal shear strain was taken as 5×10^5 kPa and the intact undrained shear strength (s_{u0}) was taken as 10 kPa, typical values for marine clays. The failure envelopes are presented as dimensionless quantities, such that the particular magnitude of soil strength selected for the analyses is not relevant, and the effect of the ratio of stiffness to strength is considered in the parametric study presented later. The main soil strain softening and rate parameters in the model include soil sensitivity (S_t), soil relative ductility (ξ_{95}) and strain rate parameter (μ) which

can deduced from soil shear strengths and accumulated absolute plastic shear strains at different cycles of strain-controlled undrained cyclic tests or cyclic penetration and extraction tests using full-flow penetrometers such as T-bar and ball according to Eq. (1) to (4). Soil sensitivity (S_t), soil relative ductility (ξ_{95}), strain rate parameter (μ) and the reference shear strain rate ($\dot{\gamma}_{ref}$) for the soil element were taken as 4, 10, 0.05 and 3×10^{-6} s^{-1} which are typical values within the recommended ranges of marine clays [14, 23-25]. For the finite element analysis, Poisson's ratio is assumed 0.49 to simulate the undrained soil conditions of no volume change while ensuring numerical stability. The second-order fully integrated brick, hybrid element C3D20H [15] is adopted. The hybrid element formulation uses a mixture of displacement and stress variables and is recommended for simulating the response of near-incompressible materials, such as undrained clay to more clearly identify the plastic yield point. Fig. 2 demonstrates the accuracy of the user subroutine of the strain softening and rate dependent constitutive model programmed for Abaqus and demonstrates the versatility of the strength degradation model for varying levels of strain. The initial value of s_u/s_{u0} is greater than 1 due to the rate effect once cyclic loading has been initiated, with the logarithmic horizontal scale starting at $N = 0.03$. The forms of the stress-strain and strength degradation responses indicate the reduction in stiffness and strength with increasing number of cycles. Good agreement between the finite element method (FEM) simulation result and the theoretical solution calculated by Eq. (1) to Eq. (4) indicates the correctness of the developed code for the user material subroutine used in this study.

The strain softening and rate dependent model adopted in this study has been validated for cyclic loading conditions through comparison with experimental results of cyclic T-bar tests [21] and dynamic pipe lay [22]. The agreement of theoretical and experimental results demonstrates that the selected model can capture the degradation characteristics of soft clay under cyclic loading. An additional validation is presented in Fig. 3, which compares strength degradation with number of cycles predicted by the constitutive model implemented in the finite element program and that reported from a cyclic simple shear test [29]. Conditions modelled in the finite element analysis

replicated those reported for the simple shear test: Symmetrical cyclic loading at a cyclic horizontal shear strain of γ_c = 15% was imposed; soil sensitivity (S_t) was equal to 7, obtained from a fall cone test; the cell pressure of the specimen was 60 kPa; the initial shearing modulus of elasticity was equal to 3.15×10^6 kPa. Soil relative ductility (ξ_{95}), strain rate parameter (μ) and intact undrained shear strength (s_{u0}) were taken as 7.67, 0.024 and 12.42 kPa respectively deduced from soil shear strengths and accumulated absolute plastic shear strains at N = 0.25, 0.75, 5.75 and 9.25 according to Eq. (1) to (3). The reference shear strain rate ($\dot{\gamma}_{ref}$) was assumed as 3×10^{-6} s^{-1}. For the finite element numerical analysis, Poisson's ratio was assumed 0.49. The FEM simulation result shows close agreement with the experimental data. The shear strain rate applied in the experimental tests from N = 0 to N = 0.25 and from N = 9 to N = 9.25 was 4.5% / hour while it was 45% / hour at the rest of the cyclic simple shear test [29]; and these different shearing rates over different time periods were replicated in the finite element analysis. According to Eq. (1) to (4), the lower the shear strain rate, which will reduce the strain rate factor (β_s), the lower the soil shear strength. The soil shear strengths at N = 0.25 and N = 9.25 of the experimental data and FEM simulation result are smaller than the predicted values observed from the fitted polynomial curves of experimental data and FEM simulation result except points at N = 0.25 and N = 9.25 because of a low shearing rate effect. The validation shows that the Tresca model modified by the Einav and Randolph model can adequately describe the soil strain softening and rate effects under cyclic loading.

4. Failure envelope of shallow foundation on intact soil

The failure envelope of a shallow foundation on intact soil is first evaluated. A two-dimensional finite element model in plane strain conditions is shown in Fig. 4. The foundation width is denoted as B and the soil domain is $12\times6B$. Infinite elements were initially considered at the periphery of the mesh as these are recommended for cyclic or dynamic loading events, but resulting failure envelopes with and without considering soil strain softening and rate effects were the same with and without infinite

elements indicating that the soil domain was sufficient to ensure no boundary effects. For computational efficiency (time and storage space), the model without infinite elements was adopted. Finer mesh discretisation (minimum element size $B/40$) is used in the region close to the foundation to improve numerical accuracy. The pure capacities on intact soil and the effect of minimum element size on the post-cyclic capacity, that are shown later, indicated that the meshes adopted in this study were optimally refined and provided a balance between accuracy and calculation efficiency. A mesh sensitivity study is presented later (in Section 5.3). The second-order fully integrated rectangular hybrid element CPE8H was adopted. The strip foundation was modelled as a rigid body with the reference point prescribed at the centre of the foundation base. The interface between the soil and the foundation was modelled as fully bonded, to represent undrained uplift resistance of the foundation, in practice achieved by passive suction (relative to ambient pressure) developed between the seabed and underside of the foundation [3], considered appropriate for the short-term cyclic loading considered in this study.

The soil was modelled as a Tresca material with a uniform intact undrained shear strength defined by s_{u0}. It is acknowledged that deep offshore sediments often exhibit linearly increasing undrained shear strength with depth. The assumption of uniform soil strength with depth for this study is an appropriate approximation for many nearshore seabeds and to demonstrate the proposed numerical method accounting for cyclic loading effects. Young's modulus $E = 1000s_u$ and Poisson's ratio was assumed 0.49.

The probe test approach, introduced by Bransby and Randolph [2], was adopted to numerically evaluate the failure envelope. In the probe test, the foundation is displaced at fixed ratios of displacements u/w, $\theta B/w$, and $\theta B/u$. Consequently, the resultant load develops until an ultimate load is reached. Fig. 5 illustrates the normalised resistance for the probe test with a displacement ratio of $u/w = 3$. By plotting the loading path in *VHM* space, the final point i.e. ultimate load, is considered to be sitting on the failure envelope. The failure envelopes are obtained by fitting a smooth curve through

the final points of all the probe tests. 26 probe tests were conducted in this analysis as illustrated in Fig. 6 to assess the failure envelopes. Also shown are the numerical results presented in Gourvenec [4], indicating close agreement with this study.

Pure vertical, horizontal and moment capacity on intact soil are defined as $V_{ult,intact}$, $H_{ult,intact}$ and $M_{ult,intact}$ respectively. The pure vertical capacity factor $N_{V,intact} = V_{ult,intact}/Bs_{u0} = 5.22$ in this study is 1.5% greater than the exact solution of $2 + \pi$ [30] while the moment capacity factor $N_{M,intact} = M_{ult,intact}/B^2s_{u0} = 0.72$ is about 4.3% greater than the upper bound solution of 0.69 proposed by Murff and Hamilton [31]. According to the assumption that sliding failure of a rough-based surface foundation occurs along the soil-foundation interface, the horizontal resistance equal to the mudline undrained shear strength and thus $N_{H,intact} = 1$. The horizontal capacity factor is calculated as $N_{H,intact} = H_{ult,intact}/Bs_{u0} = 1.06$ in this study, which is slightly greater (6%) than the exact solution of 1.0. These comparisons indicate that the finite element model for this study is acceptably accurate.

5. Evolution of failure envelope under cyclic loading

5.1 Example case study

Geometry and loading conditions

An example is presented in this section to illustrate the proposed methodology for capturing the effects of soil degradation resulting from multi-directional cyclic loading on the undrained failure envelope for a shallow foundation. The example is based on a proposed caisson breakwater with smooth curved face, shown in Fig. 7, to be installed off the coast of Tianjin, China. The breakwater has a foundation width $B = 29$ m. The seabed was found to have a uniform initial (intact) soil shear strength $s_{u0} = 20$ kPa within the depth of interest. The wave forces acting on the curved face provide horizontal and vertical load components on the foundation. Meanwhile, the base stress under a caisson breakwater with a curved face is more uniform than for a traditional caisson breakwater with a vertical wall. Thus this kind of caisson breakwater is suitable for more severe wave conditions

compared with a traditional caisson breakwater with a vertical wall. The submerged self-weight of the foundation and superstructure (W') is taken as 1515 kN/m, which amounts to $W'/Bs_{u0} = V_{ult,intact}/Bs_{u0}/2 = N_{V,intact}/2$. Cyclic environmental loads, such as a storm loading, can be idealised as a sinusoidal cyclic sequence [32] This study takes the cyclic load period T as 6 seconds and a 100 minute storm is considered (i.e. 1000 cycles of sinusoidal loading). A cyclic amplitude of $0.3V_{ult,intact}$ around the self-weight W' and cyclic amplitudes of $0.6H_{ult,intact}$ and $0.6M_{ult,intact}$ about a zero horizontal load or moment are considered. As illustrated in Fig. 8, the vertical load cycles about the self-weight W' vary between $0.35V_{ult,intact}$ and $0.65V_{ult,intact}$; the horizontal load cycles between $-0.3H_{ult,intact}$ and $0.3H_{ult,intact}$ and moment from $-0.3M_{ult,intact}$ and $0.3M_{ult,intact}$. As V, H and M have the same phase, the loading path represents a straight line in VHM space. It is acknowledged that the load path during a storm can be much more complex than this linear assumption. However, this study focussed on demonstrating the proposed method to investigate the evolution of failure envelopes - the methodology can be applied to consider any combination of cyclic loading.

Soil conditions

The Tresca criterion modified by the Einav and Randolph model as outlined and validated above was adopted to model the soil response. In the current example, soil sensitivity, soil relative ductility, strain rate parameter and the reference shear strain rate were chosen with $S_t = 4$, $\xi_{95} = 30$, $\mu = 0.1$ and $\dot{\gamma}_{ref} = 3\times10^{-6}\ s^{-1}$, respectively. The values fall within the range of suggested values for marine clays [14, 23-25], derived from the test methods described in Section 3.2. A sensitivity study of the various model parameters is presented in section 6. Analysis methodology

The combined approach of load controlled geometrically nonlinear finite element analysis and displacement controlled small strain finite element analysis described in section 3 and 4 was used. Initially multi-directional VHM cyclic loading was applied in a geometrically nonlinear finite element analysis during which process the gradual evolution of the shear strength due to soil strain softening and rate effects under multi-directional cyclic loading is captured. In order to obtain the gradual

evolution of the shear strength due to soil strain softening and rate effects under multi-directional cyclic loading, load controlled geometrically nonlinear finite element analyses are adopted. In order to evaluate the capacity of a shallow foundation after the action of multi-directional cyclic loading considering soil degradation, monotonic displacement controlled probe tests were carried out to evaluate the failure envelope based on the updated shear strength field of the soil, which is passed from the result of the load controlled geometrically nonlinear finite element analysis.

Monotonic displacement controlled probe tests were carried out to evaluate the failure envelope at N = 0, 200, 600 and 1000 cycles of loading (N = 0 corresponds to an intact soil response). The Young's modulus (E) is directly related to s_u through a constant E/s_u ratio (1000 unless otherwise specified) and Poisson's ratio is assumed 0.49. The undrained shear strength s_u is related to the field variable, which is specified as an initial condition prior to the probe test analyses.

5.2 Degradation of undrained shear strength s_u across the soil domain

The soil strain softening factor (β_s) under multi-directional cyclic loading is plotted as contour lines in Fig. 9 corresponding to cycle number N = 200, 600, 1000. Low β_s indicates a high degree of degradation and thus lower soil undrained shear strength (s_u). Fig. 9 indicates the greatest degradation of soil shear strength due to plastic shear strain is concentrated in soil elements at one corner of the foundation. The extent of the zone of soil degradation increased with increasing number of loading cycles and the asymmetrical soil degradation zones are due to the coupled effect of cyclic *VHM* loading.

Fig. 10 reiterates the non-uniform soil degradation across the soil domain, showing strain softening factor and accumulated absolute plastic shear strain at four discrete integration points in the soil domain close to the foundation. Points A and D are located under the right corner of the strip foundation at a depth of 0.025B and 0.2B respectively, while point C is located under the middle and E under the left corner of the foundation at a depth of 0.025B. From Fig. 10, we can see that soil strain softening factor (β_s) calculated by the finite element method has the same value as that calculated by

Eq. (2), providing an additional check for the user subroutine developed for the finite element program. Integration point *A*, which is located at the compressive corner at shallow depth, has minimum values of soil strain softening factor (β_s), i.e. greatest degradation in soil strength, and the maximum values of accumulated absolute plastic shear strain (ξ). The soil at point *A* has been almost completely remoulded after 1000 cycles. Integration point *C*, which is located under the middle of the strip foundation, has the maximum value of soil strain softening factor (β_s) , i.e. minimum degradation in soil strength, and the minimum value of accumulated absolute plastic shear strain (ξ). The soil at point *C* has been partially remoulded, 7.05% after 1000 cycles. Corresponding values at integration point *E* and *D* fall in between those of integration point *A* and *C*. The asymmetric soil strength degradation arises as the vertical cyclic load fluctuates around the submerged self-weight of the foundation and superstructure (W'), such that the base stresses during the first half of every cycle are higher than those during the latter half according to Fig. 8. As a result, the shallow foundation rotates towards integration point *A* due to the moment loading during the first half of every cycle while to integration point *E* during the latter half. Accumulated absolute plastic shear strain (ξ) at integration point *A* is higher than that at point *E*, because the shallow foundation rotates to integration point *A* with a higher soil stress due to the vertical loading while to integration point *E* with a lower soil stress. So point *A* has a smaller value of soil strain softening factor (β_s) than point *B*.

5.3 *Effect of cyclic preloading on failure envelopes*

Failure envelopes in *VH*, *VM* and *HM* planes at N = 0, 200, 600, 1000 are illustrated in Fig. 11, where N = 0 indicates the intact soil case. This figure shows that capacity reduces, indicated by the failure envelopes contracting inward, with increasing number of loading cycles as the extent and magnitude of soil strength degradation increases. Pure vertical, horizontal and moment capacity are defined as V_{ult}, H_{ult} and M_{ult}, respectively. In this example, the vertical capacity factor Nv = V_{ult}/Bs_{u0}, horizontal capacity factor $N_H = H_{ult}/Bs_{u0}$ and the moment capacity factor $N_M = M_{ult}/B^2s_{u0}$ decreased by 5.49%, 6.96% and 6.46%, respectively after 1000 cycles of loading compared with pure vertical, horizontal

and moment capacity on intact soil (i.e. $N_{V,intact}$, $N_{H,intact}$ and $N_{M,intact}$). It is noted that both strain softening and rate effects are accounted for during the cyclic pre-loading in the load controlled geometrically nonlinear finite element analysis. Displacement controlled probe tests were carried out to obtain the undrained failure envelope which can be used to evaluate the capacity of a shallow foundation after the action of multi-directional cyclic loading considering soil degradation. The rate enhancement effect is neglected to obtain the undrained failure envelope since shear strain rate is not considered in the displacement controlled probe tests without cyclic loading.

The shape of the failure envelope following a sequence of multi-directional cyclic loading is quite consistent despite the asymmetric degradation zone. Thus, it is reasonable to scale the failure envelope by only using the pure capacities V_{ult}, H_{ult}, M_{ult}, while assuming the shape of the envelope is constant. Vertical, horizontal and moment capacity reduction factors, α_V, α_H and α_M, defined as $V_{ult}/V_{ult,intact}$, $H_{ult}/H_{ult,intact}$ and $M_{ult}/M_{ult,intact}$ respectively can be defined to scale the envelopes. This is shown in Fig. 12, 14, 16, 18, 20 and 21 later for the specific loading protocol considered in this study. The lower the values of pure capacity reduction factors α_V, α_H and α_M, the greater the soil degradation and hence reduction in capacity.

Mesh sensitivity analyses were carried out with 3 different meshes characterised by different minimum element sizes to ensure optimal calculation accuracy. Minimum element sizes of 0.01*B*, 0.025*B* (selected for this study) and 0.05*B* were considered. It can be indicated from Fig. 12 that the post-cyclic capacities of shallow foundations with different minimum element sizes show a close agreement. The maximum error is less than 1.1%. The results indicate that the meshes adopted in this study are suitably refined.

5.4 Effect of cyclic preloading on failure mechanisms

The plastic shear bands (which are a reasonable measure to represent the failure mechanism) corresponding to the pure vertical probe test at N = 0, 200, 600, 1000 of *VHM* cyclic loading are shown in Fig. 13. The failure mechanism under pure vertical load, following cyclic *VHM* preloading,

gradually changed from a symmetrical "two-sided" Prandtl failure mechanism to an asymmetric "one-sided" mechanism due to non-uniform evolution of undrained shear strength across the soil domain with weaker soil around one corner (as also shown in Fig. 9).The development of asymmetric strength degradation is discussed in section 5.2, and is caused by the coupled effect of cyclic *VHM* loading. A failure zone will preferentially generate in soil with lowest undrained shear strength, following the path of least resistance. Increasingly weaker undrained shear strength of the soil near one corner of the foundation is responsible for the transition of the failure mechanism from a symmetrical two-sided configuration to an asymmetric one-sided configuration.

It is found that the failure mechanisms under pure horizontal sliding and pure rotation post cyclic loading are both largely unchanged in this example. The failure mechanism under pure horizontal loading is still a translational sliding mechanism beneath the foundation while a scoop mechanism governs under pure moment. Thus plots of plastic shear bands at failure under a pure horizontal sliding and pure rotation probe following cyclic loading are omitted for brevity.

6. Parametric study of model parameters

A parametric study was carried out to assess the effects of the value of strain softening and rate parameters including soil sensitivity, S_t, relative ductility, ξ_{95} and strain rate parameter, μ, the stiffness index, E/s_u and the period of cyclic loading, T. All parameters were kept the same as the "base case" calculation example presented above, with only one parameter varying in any individual parametric analysis.

6.1 Effect of soil sensitivity, S_t

Three values of soil sensitivity, S_t = 2, 4 (base case), 6 were considered. Clays with a higher value of soil sensitivity, S_t are prone to experience a greater loss of strength as a result of remoulding. Effects of the magnitude of soil sensitivity, S_t, on capacity reduction of α_V, α_H and α_M are shown in Fig. 14. It is evident that the degree of degradation of pure capacity increases with increasing number of loading cycles (N) due to the steady accumulation of absolute plastic shear strain. Further, greater sensitivity

S_t results in greater reduction in capacity of a coastal and offshore shallow foundation following a sequence of undrained cyclic loading considering soil degradation. Effects of the magnitude of soil sensitivity, S_t on degradation factor β_s of shear strength s_u when N = 1000 are shown in Fig. 15. The extent of the zone of soil degradation increased with increase of soil sensitivity, S_t, which causes greater reduction in capacity of a shallow foundation on a deposit with greater sensitivity S_t.

6.2 Effect of soil relative ductility, ξ_{95}

Three values of soil relative ductility, ξ_{95} = 10, 30 (base case), 50 were considered. A more ductile clay has a higher value of soil relative ductility, ξ_{95} while a more brittle clay has a lower value. Effects of the magnitude of soil relative ductility, ξ_{95} on capacity reduction factors α_V, α_H and α_M are shown in Fig. 16. Effects of the magnitude of soil ductility parameter, ξ_{95} on degradation factor β_s of shear strength s_u when N=1000 are shown in Fig. 17. Values of α_V, α_H and α_M reduce with increasing number of load cycles (N). Greater soil ductility parameter, ξ_{95} obviously reduces the extent of the zone of soil degradation, so greater soil relative ductility ξ_{95} effectively reduces the softening. Physically, brittle clay tends to have greater reduction in capacity than ductile clay following the sequence of cyclic loading.

6.3 Effect of soil strain rate parameter, μ

Three values of soil strain rate parameter, μ = 0.05, 0.10 (base case), 0.2 were considered. Clays with a higher value of soil strain rate parameter, μ have a stronger rate effect, associated with higher enhancement in undrained shear strength with rate. Effects of the magnitude of soil strain rate parameter, μ on capacity reduction factors α_V, α_H and α_M are shown in Fig. 18. Effects of the magnitude of soil rate parameter, μ on degradation factor β_s of shear strength s_u when N=1000 are shown in Fig. 19. Values of α_V, α_H and α_M reduce with increasing number of load cycle N. Larger soil rate parameter, μ reduces the extent of the zone of soil degradation and tends to enhance soil strength and thus less plastic strain is accumulated with increasing number of load cycles (N). Consequently,

less capacity reduction can be seen for greater μ.

6.4 Effect of constant stiffness index, E/s_u

The bearing capacity of a surface foundation on a Tresca material is generally accepted to be independent of the magnitude of stiffness index, E/s_u due to the elastic perfectly plastic constitutive law. However, stiffness index (E/s_u) affects plastic strain accumulation during the cyclic loading in this study. Clays with a lower value of soil stiffness index, E/s_u have a higher compressibility. Parametric analyses with stiffness indicies E/s_u = 500, 1000 (base case) and 1500 were considered. The result is shown in Fig. 20. It can be seen that vertical, horizontal and moment capacity reduction factors, i.e. α_V, α_H and α_M, decreased with increasing number of loading cycles (N). Larger E/s_u (stiffer soil) leads to less shear strain and thus less degradation, such that a greater reduction in capacity of coastal and offshore shallow foundation on clays with high compressibility would be expected following a sequence of cyclic loading considering soil degradation.

6.5 Effect of period of cyclic loading, T

Three periods of cyclic loading, T = 3.6, 6 (base case), 12 s were considered. A lower period of cyclic loading, T generates a larger shear strain rate and has a stronger rate effect, leading to a higher enhancement in undrained shear strength with rate. Effects of the magnitude of period of cyclic loading, T on capacity reduction factors α_V, α_H and α_M are shown in Fig. 21. Values of α_V, α_H and α_M reduce with increasing number of load cycle N. Smaller T tends to enhance soil strength and thus less plastic shear strain is accumulated with increasing number of load cycles N. Consequently, less capacity reduction can be seen for smaller T although the effect is minimal.

In summary, results of the parametric analyses have shown that soil sensitivity, S_t, relative ductility, ξ_{95} and the stiffness index, E/s_u have more influence on capacity of shallow foundations subjected to undrained cyclic preloading than strain rate parameter, μ and the period of cyclic loading, T.

7. Concluding Remarks

A practical method has been presented to evaluate failure envelopes of coastal and offshore shallow foundations considering soil strain softening and rate effects under cyclic loading. This method is realised through a user subroutine in the finite element software ABAQUS, using a combined approach of load controlled geometrically nonlinear finite element analysis and displacement controlled small strain finite element analysis. The method can be applied to a range of different coastal and offshore shallow foundation conditions, and to large deformation problems using the RITSS FEM approach.

Soil degradation is detrimental to the capacity of shallow foundations and should be taken into account in design of coastal and offshore shallow foundations. The method presented in this paper captures significant reductions in undrained capacity of coastal and offshore shallow foundations on saturated marine clays following a sequence of undrained multi-directional cyclic loading, by considering soil strength degradation in the constitutive model. The kinematic mechanisms accompanying failure under pure vertical probe tests were shown to change significantly due to the resulting non-uniform undrained shear strength across the soil domain following a sequence of multi-directional cyclic loading.

This study considers the soil response as fully undrained, i.e. ignoring any gain in soil strength due to soil consolidation as a safety reserve. The method presented here offers a rational and practical way to account for soil strength degradation due to the combined effects of strain softening and rate effects by incorporating the Einav and Randolph model for strain softening and rate effects into a Tresca model. The Einav and Randolph model has less parameters than other strength degradation models, and the parameters have clear physical meaning and can be easily obtained from soil strain-controlled undrained cyclic tests or cyclic penetration and extraction tests with flow around penetrometers. The undrained soil response modelled saves computational cost as pore pressures do not need to be calculated in each step. The method is practical and appropriate to evaluation of the undrained post-cyclic capacity of coastal and offshore shallow foundations.

Acknowledgements

A big part of this work was carried out while the first author was a visiting scholar at the Centre for Offshore Foundation Systems (COFS), with acknowledgements of the support of the National Natural Science Foundation of China (Grant No. 51479133 and 51109157), the Science Fund for Creative Research Groups of the National Natural Science Foundation of China (Grant No. 51321065) and the State Scholarship Fund of China Scholarship Council (CSC). This study comprises part of the activities of State Key Laboratory of Hydraulic Engineering Simulation and Safety of Tianjin University with the open funding (HESS-1504) is much appreciated. This work also forms part of the activities of the Centre for Offshore Foundation Systems (COFS). Established in 1997 under the Australian Research Council's Special Research Centres Program, COFS is supported as a node of the Australian Research Council's Centre of Excellence for Geotechnical Science and Engineering, and through the Fugro Chair in Geotechnics, the Lloyd's Register Foundation Chair and Centre of Excellence in Offshore Foundations and the Shell EMI Chair in Offshore Engineering. The Lloyd's Register Foundation helps to protect life and property by supporting engineering-related education, public engagement and the application of research. The third author is supported through ARC grant CE110001009. This support is gratefully acknowledged.

548 REFERENCES

549 [1.] Roscoe KH, Schofield AN. The stability of short pier foundations in sand: discussion. Br. Weld. J. 1957; 12–18.

550 [2.] Bransby MF, Randolph MF. Shallow foundations subject to combined loadings. In: Proceedings of the 9th
551 International Conference on Computer Methods and Advances in Geomechanics, Wuhan, China. 1997, pp. 1947–
552 1952.

553 [3.] Taiebat HA, Carter JP. Numerical studies of the bearing capacity of shallow foundations on cohesive soil subjected to
554 combined loading. Géotechnique 2000; 50(4): 409–418.

555 [4.] Gourvenec S. Shape effects on the capacity of rectangular footings under general loading. Géotechnique 2007; 57(8):
556 637–646.

557 [5.] Barari A, Ibsen LB. Undrained response of bucket foundations to moment loading. Applied Ocean Research 2012;
558 36: 12–21.

559 [6.] Hung LC, Kim SR. Evaluation of combined horizontal-moment bearing capacities of tripod bucket foundations in
560 undrained clay. Ocean Engineering 2014; 85: 100-109.

561 [7.] Bransby MF. The undrained inclined load capacity of shallow foundations after consolidation under vertical loads. In
562 Numerical models in geomechanics: proceedings of the 8th international symposium (NUMOG VIII), Rotterdam, the
563 Netherlands. 2002, pp. 431–437.

564 [8.] Feng X, Gourvenec S. Consolidated undrained load-carrying capacity of subsea mudmats under combined loading in
565 six degrees of freedom. Géotechnique 2015; 65(7): 563-575.

566 [9.] Andersen KH, Lauritzsen R. Bearing capacity for foundations with cyclic loads. Journal of Geotechnical Engineering
567 ASCE 1988; 114(5): 540–555.

568 [10.] Chen W, Randolph MF. Uplift Capacity of Suction Caissons under Sustained and Cyclic Loading in Soft Clay.
569 Journal of Geotechnical and Geoenvironmental Engineering ASCE 2007; 133(11): 1352–1363.

570 [11.] Liyanapathirana DS. Arbitrary Lagrangian Eulerian based finite element analysis of cone penetration in soft clay.
571 Computers and Geotechnics 2009; 36(5): 851-860.

572 [12.] Mortezaie AR, Vucetic M. Effect of frequency and vertical stress on cyclic degradation and pore water pressure in
573 clay in the NGI simple shear device. Journal of Geotechnical and Geoenvironmental Engineering ASCE 2013;
574 139(10): 1727–1737.

575 [13.] Yan S, Liu R, Fan Q, Xie S. Stability of the guiding dike in Yangtze estuary under the wave load. China Ocean
576 Engineering 2005; 19(4): 659–670.

[14.] Einav I, Randolph MF. Combining upper bound and strain path methods for evaluating penetration resistance. International Journal for Numerical Methods in Engineering 2005; 63(14): 1991-2016.

[15.] Abaqus user's manual, version 6.13; 2013.

[16.] Zhou J, Gong X. Strain degradation of saturated clay under cyclic loading. Canadian Geotechnical Journal 2001; 38(1): 208–212.

[17.] Allotey N, El Naggar MH. A consistent soil fatigue framework based on the number of equivalent cycles. Journal of Geotechnical and Geological Engineering ASCE 2008; 26(1): 65–77.

[18.] Huang M, Liu Y, Sheng D. Simulation of yielding and stress–stain behavior of shanghai soft clay. Computers and Geotechnics 2011; 38(3): 341–353.

[19.] Hu C, Liu H, Huang W. Anisotropic bounding-surface plasticity model for the cyclic shakedown and degradation of saturated clay. Computers and Geotechnics 2012; 44, 34–47.

[20.] Chatterjee S, Mana DSK, Gourvenec S, Randolph MF. Large-Deformation Numerical Modeling of Short-Term Compression and Uplift Capacity of Offshore Shallow Foundations. Journal of Geotechnical and Geoenvironmental Engineering ASCE 2014; 140(3): 04013021-1–10.

[21.] Zhou H, Randolph MF. Numerical investigations into cycling of full-flow penetrometers in soft clay. Géotechnique 2009; 59(10): 801–812.

[22.] Cheuk CY, White DJ. Modelling the dynamic embedment of seabed pipelines. Géotechnique 2011; 61(1): 39–57.

[23.] Randolph MF. Characterization of soft sediments for offshore applications. In: Proc., 2nd Int. Conf. on Site Characterization, Millpress Science, Rotterdam, Netherlands. 2004, pp. 209–231.

[24.] Biscontin G, Pestana JM. Influence of peripheral velocity on vane shear strength of an artificial clay. Geotechnical Testing Journal 2001; 24(4): 423–429.

[25.] Lunne T, Andersen KH. Soft clay shear strength parameters for deepwater geotechnical design. Proceedings of the 6th International Offshore Site Investigation and Geotechnics Conference: Confronting New Challenges and Sharing Knowledge, Society for Underwater Technology, London, UK. 2007, pp. 151–176.

[26.] Gao F, Wang N, Zhao B. Ultimate bearing capacity of a pipeline on clayey soils: Slip-line field solution and FEM simulation. Ocean Engineering 2013; 73: 159–167.

[27.] Zhou H, Liu HL, Kong GQ, Huang X. Analytical solution of undrained cylindrical cavity expansion in saturated soil under anisotropic initial stress. Computers and Geotechnics 2014; 55: 232–239.

[28.] Wu K, Fan Q, Zheng J. Effect of strength anisotropy on failure envelope of offshore shallow foundations under combined loading. Journal of Coastal Research 2015; Special Issue 73: 521–526.

607 [29.] Andersen KH. Cyclic soil parameters for offshore foundation design. In: Proceeding of international symposium on
608 frontiers in Offshore Geotechnics: ISFOG, Oslo, Norway. 2015, pp. 5–82.
609 [30.] Prandtl L. Eindringungsfestigkeit und festigkeit von schneiden. Zeit. f. Angew. Math. u. Mech. 1921; 1(1):15–20.
610 [31.] Murff JD, Hamilton JM. P-ultimate for undrained analysis of laterally loaded piles. Journal of the Geotechnical
611 Engineering Division, ASCE 1993; 119 (1): 91–107.
612 [32.] Lin P. Numerical modeling of water waves. London: Taylor & Francis Co.; 2008.

613 Figure captions

614 Figure 1: Sign convention and nomenclature for loads and displacements

615 Figure 2: (a) Stress-strain response and (b) degradation of shear strength of a soil element corresponding to
616 different amplitudes of cyclic horizontal shear strain

617 Figure 3: Comparison of the soil shear strengths with number of cycles between FEM simulation result and
618 experimental data

619 Figure 4: Finite element mesh

620 Figure 5: Example of normalised load-displacement curves showing definition of failure

621 Figure 6: Validation: Failure envelopes and displacement-controlled load paths for a surface strip foundation
622 on intact soil

623 Figure 7: Cross-section diagram of the caisson breakwater with smooth curved face

624 Figure 8: Sinusoidal cyclic loading with a period T = 6 s

625 Figure 9: Contours of degradation factor β_s of shear strength s_u due to soil strain softening under undrained
626 cyclic loading

627 Figure 10: The non-uniform soil degradation at different integration points (a) Locations of integration points A,
628 C, D and E and (b) soil strain softening factors and accumulated absolute plastic shear strains at those
629 integration points

630 Figure 11: Influence of cyclic loading induced soil degradation on failure envelopes

631 Figure 12: Effect of minimum element size on post-cyclic capacity

632 Figure 13: Plastic shear bands at failure under a pure vertical displacement probe following N cycles of
633 undrained cyclic loading

634 Figure 14: Effect of soil sensitivity, S_t on post-cyclic capacity

635 Figure 15: Effect of soil sensitivity, S_t on degradation factor β_s of shear strength s_u when N=1000

636 Figure 16: Effect of soil ductility parameter, ξ_{95} on post-cyclic capacity

637 Figure 17: Effect of soil ductility parameter, ξ_{95} on degradation factor β_s of shear strength s_u when N=1000

638 Figure 18: Effect of soil rate parameter, μ on post-cyclic capacity

639 Figure 19: Effect of soil rate parameter, μ on degradation factor β_s of shear strength s_u when N=1000

640 Figure 20: Effect of stiffness index, E/S_u on post-cyclic capacity

641 Figure 21: Effect of period of cyclic loading, T on post-cyclic capacity

642

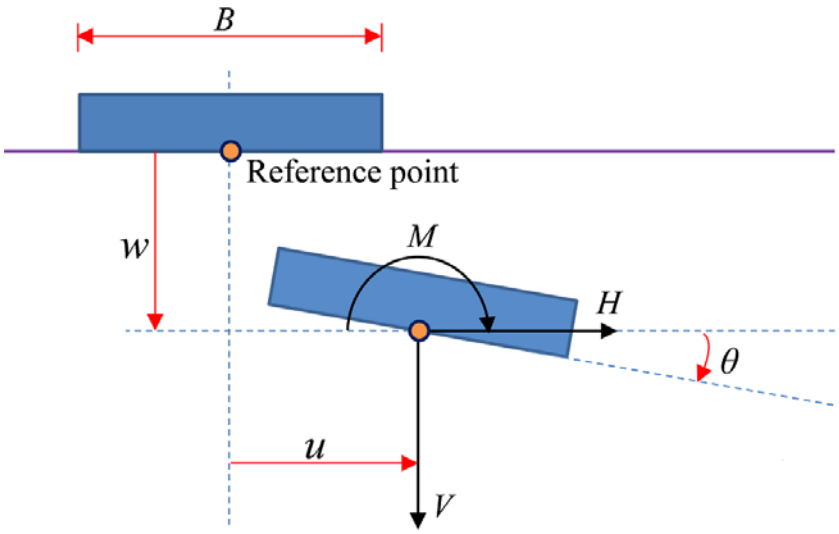

Fig. 1 Sign convention and nomenclature for loads and displacements

643

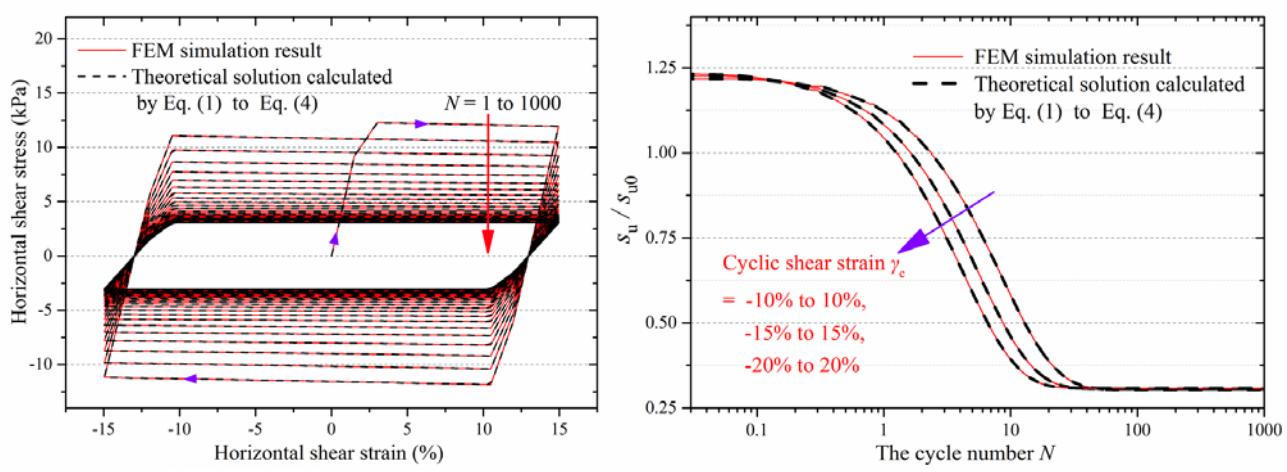

Fig. 2 (a) Stress-strain response and (b) degradation of shear strength of a soil element corresponding to different amplitudes of cyclic horizontal shear strain

644

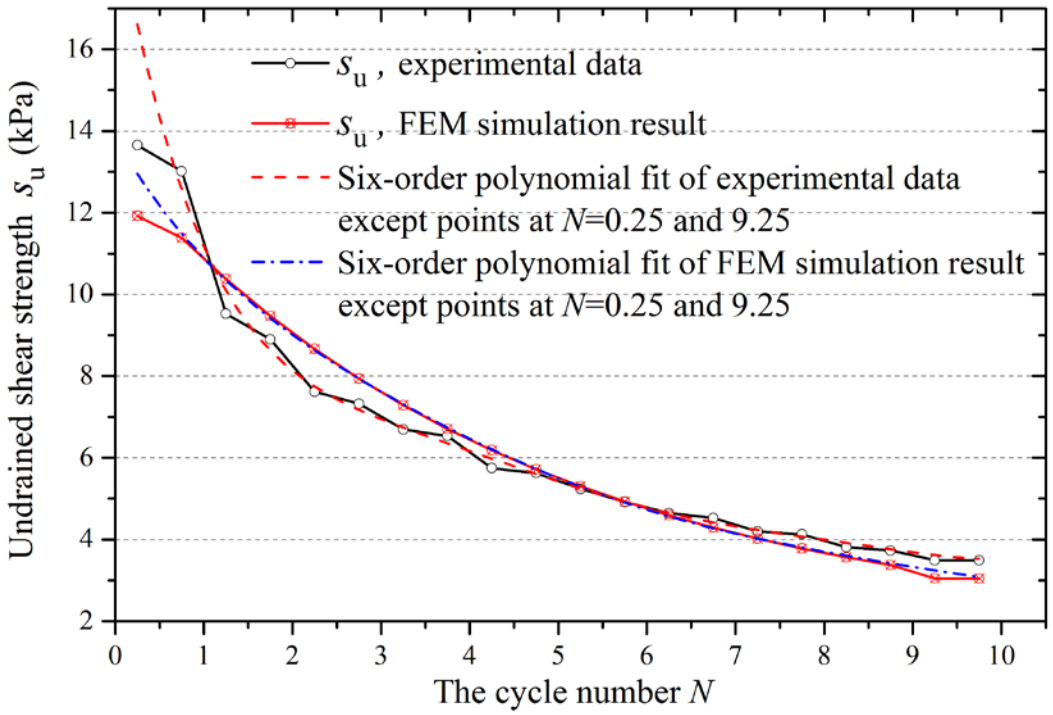

Fig. 3 Comparison of the soil shear strengths with number of cycles between FEM simulation result and experimental data

645

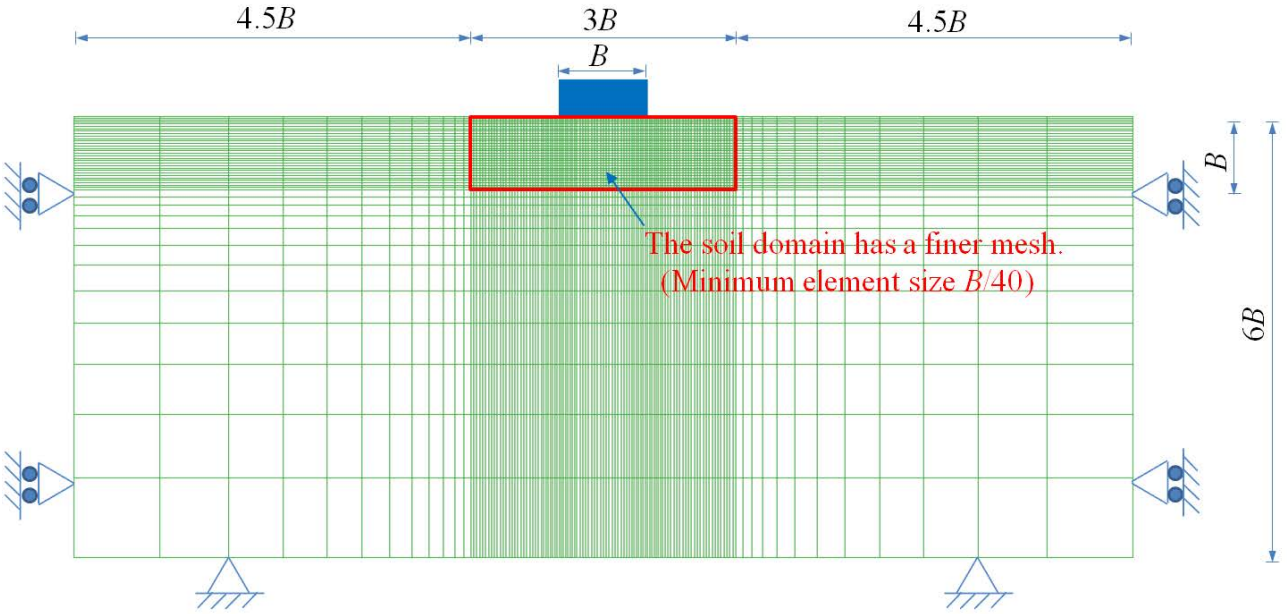

Fig. 4 Finite element mesh

646

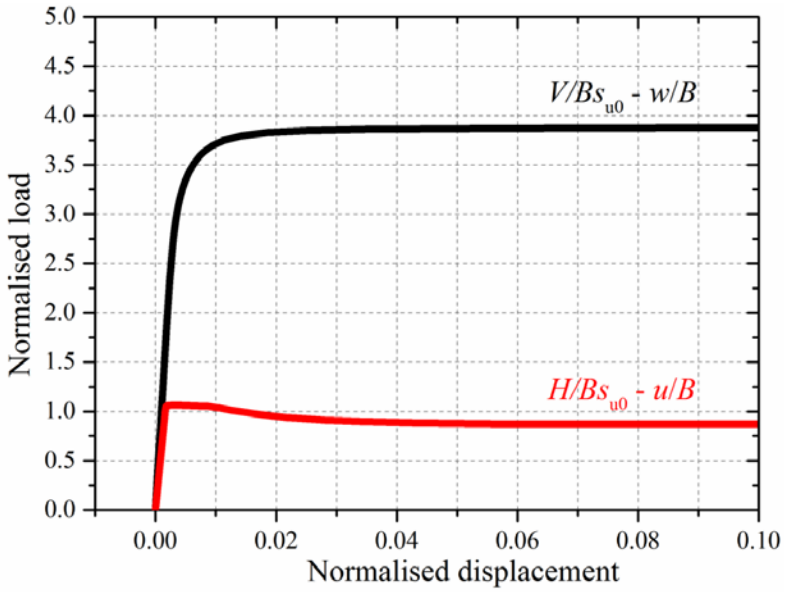

Fig. 5 Example of normalised load-displacement curves showing definition of failure

647

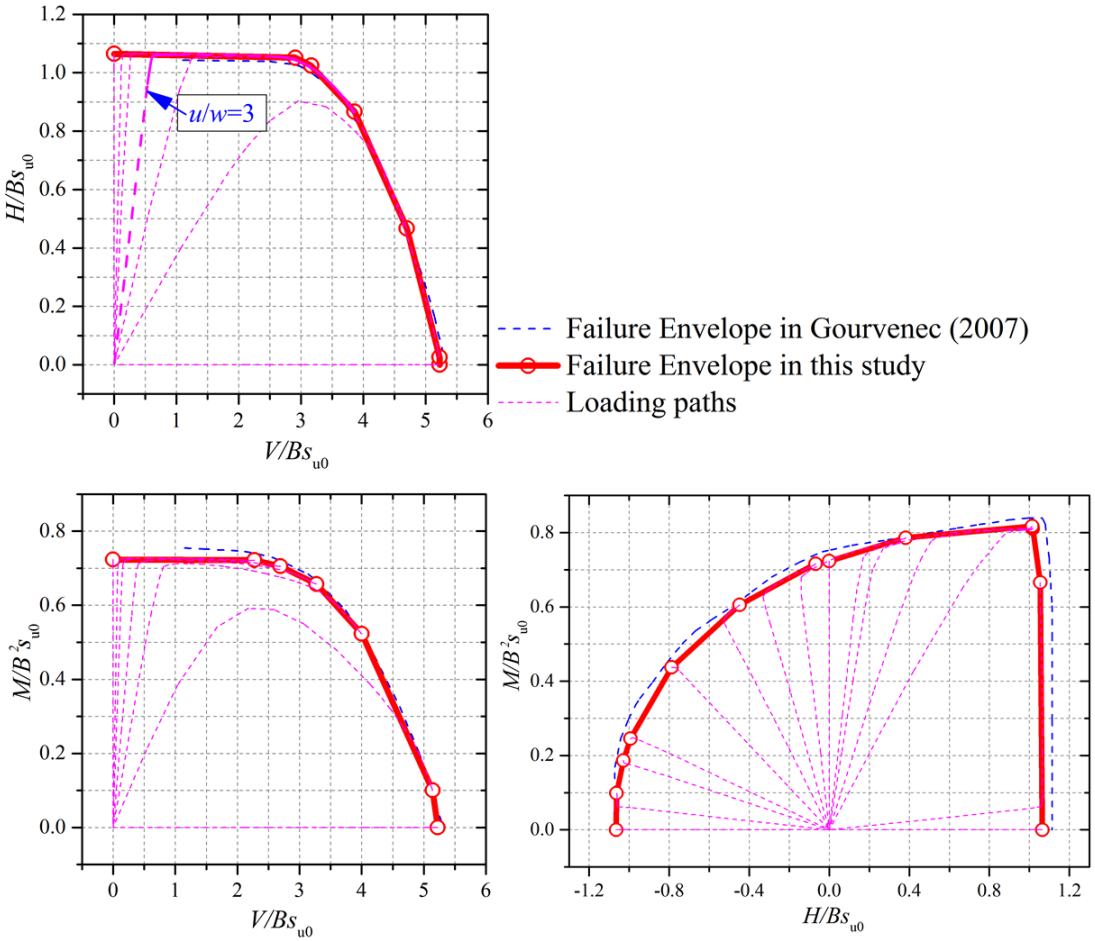

Fig. 6 Validation: Failure envelopes and displacement-controlled load paths for a surface strip foundation on intact soil

648

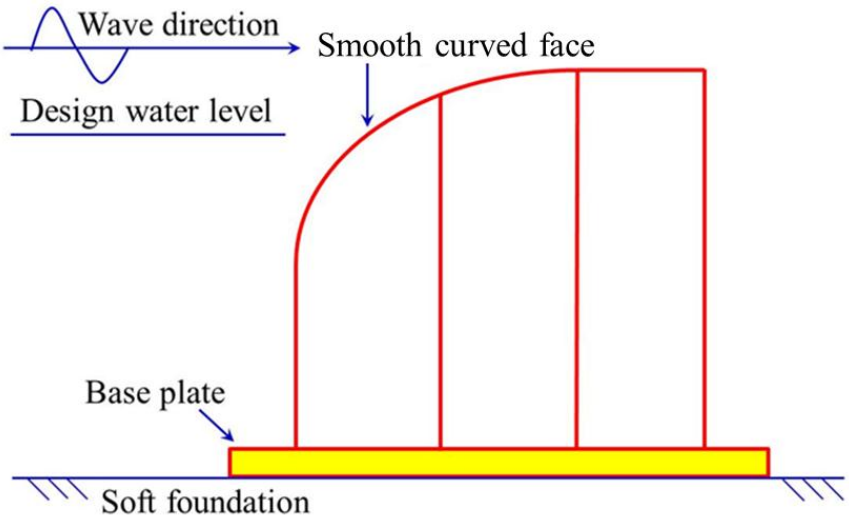

Fig. 7 Cross-section diagram of the caisson breakwater with smooth curved face

649

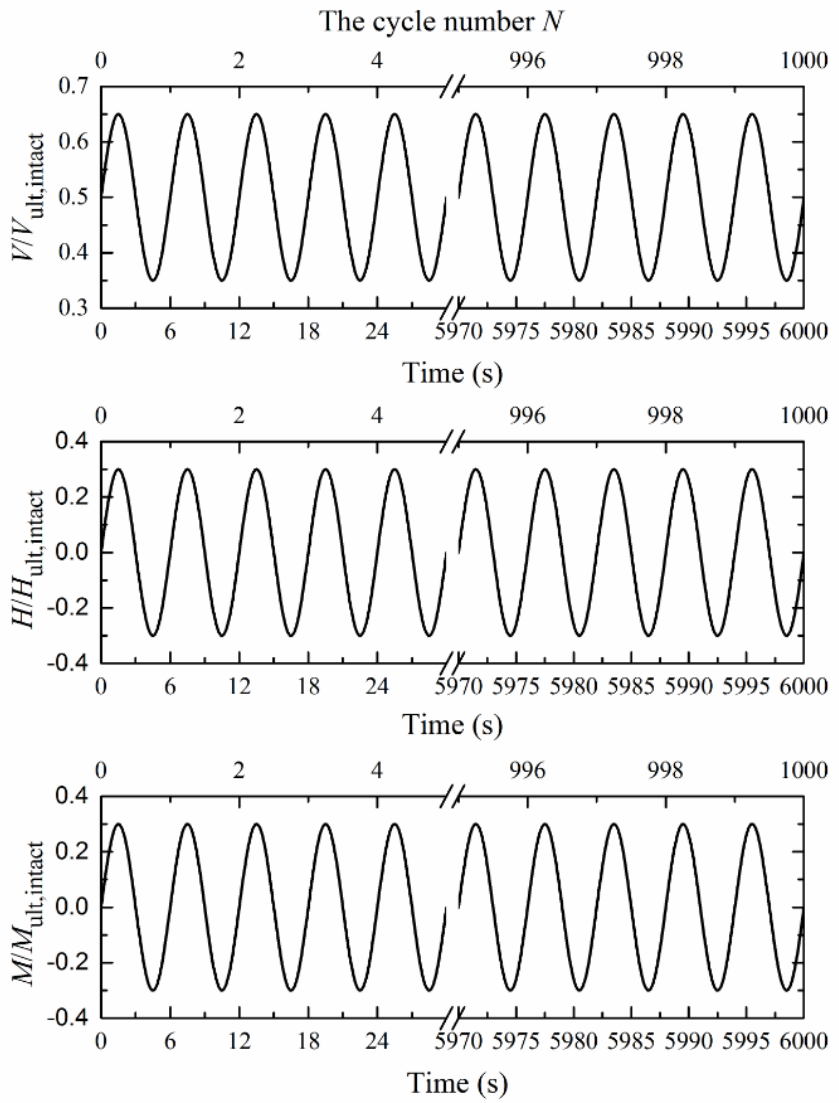

Fig. 8 Sinusoidal cyclic loading with a period T = 6 s

650

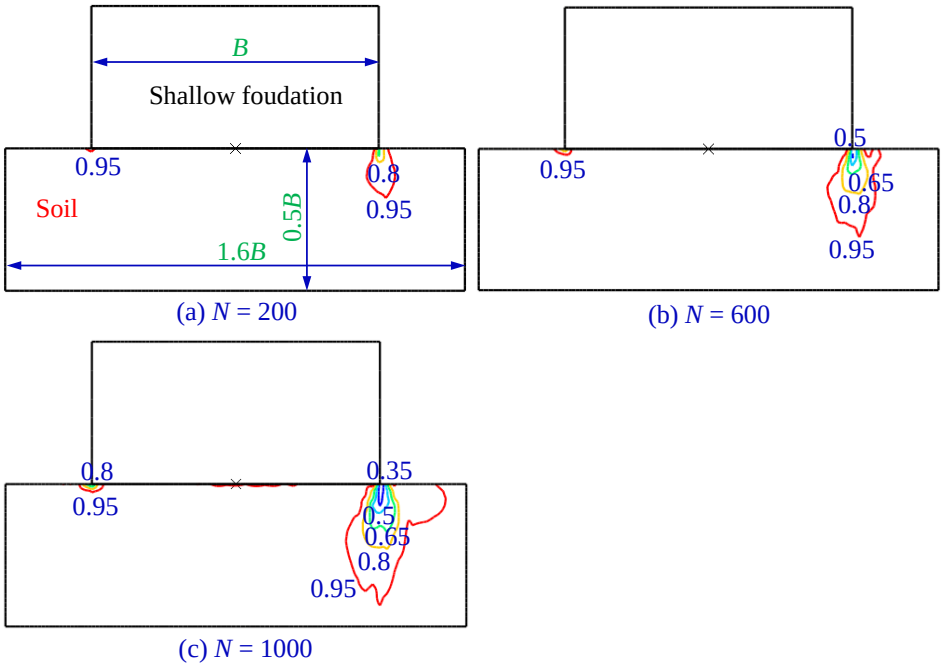

Fig. 9 Contours of degradation factor β_s of shear strength s_u due to soil strain softening under undrained cyclic loading

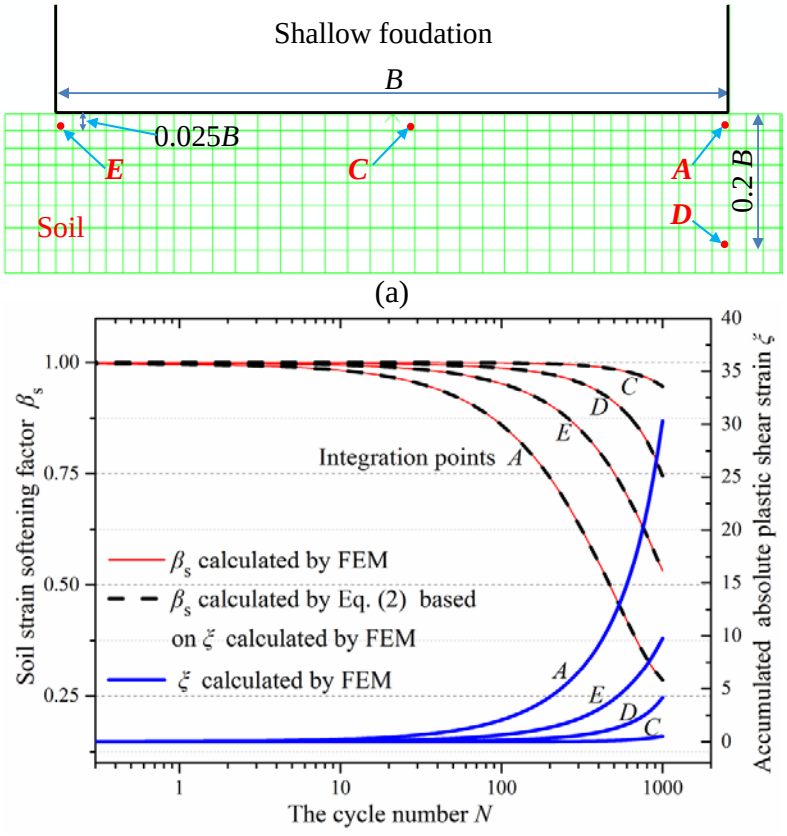

Fig. 10 The non-uniform soil degradation at different integration points (a) Locations of integration points *A*, *C*, *D* and *E* and (b) soil strain softening factors and accumulated absolute plastic shear strains at those integration points

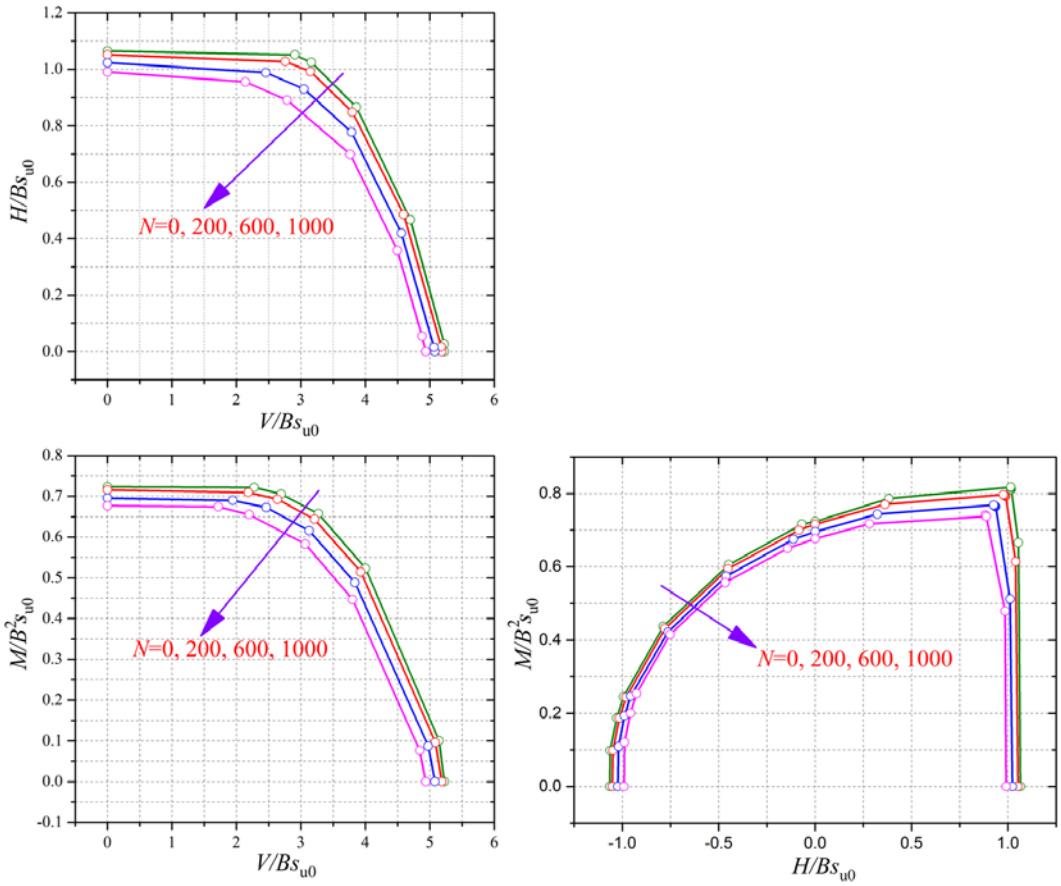

Fig. 11 Influence of cyclic loading induced soil degradation on failure envelopes

653

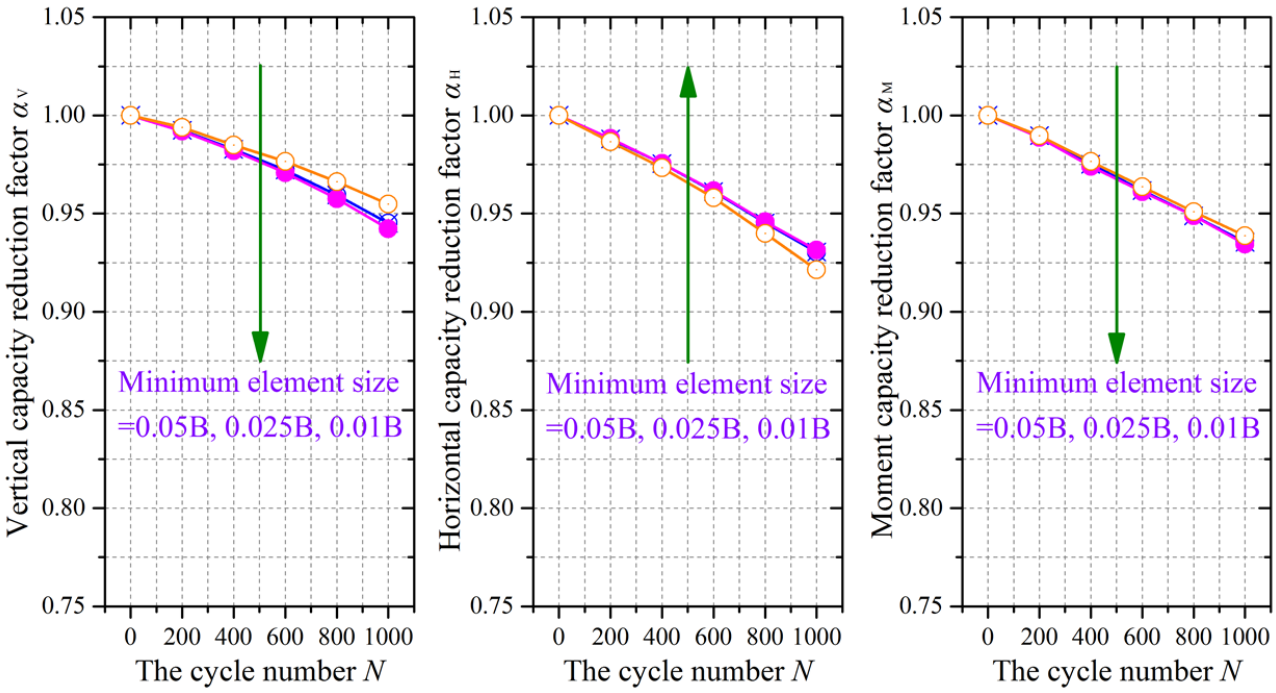

Fig. 12 Effect of minimum element size on post-cyclic capacity

654

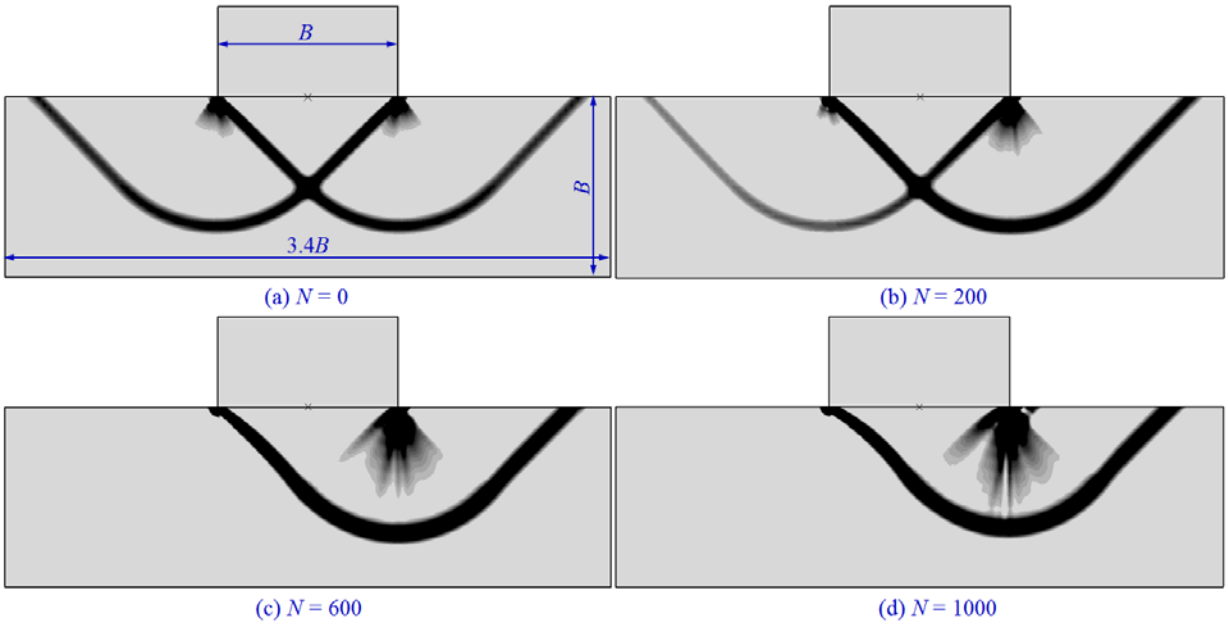

Fig. 13 Plastic shear bands at failure under a pure vertical displacement probe following N cycles of undrained cyclic loading

655

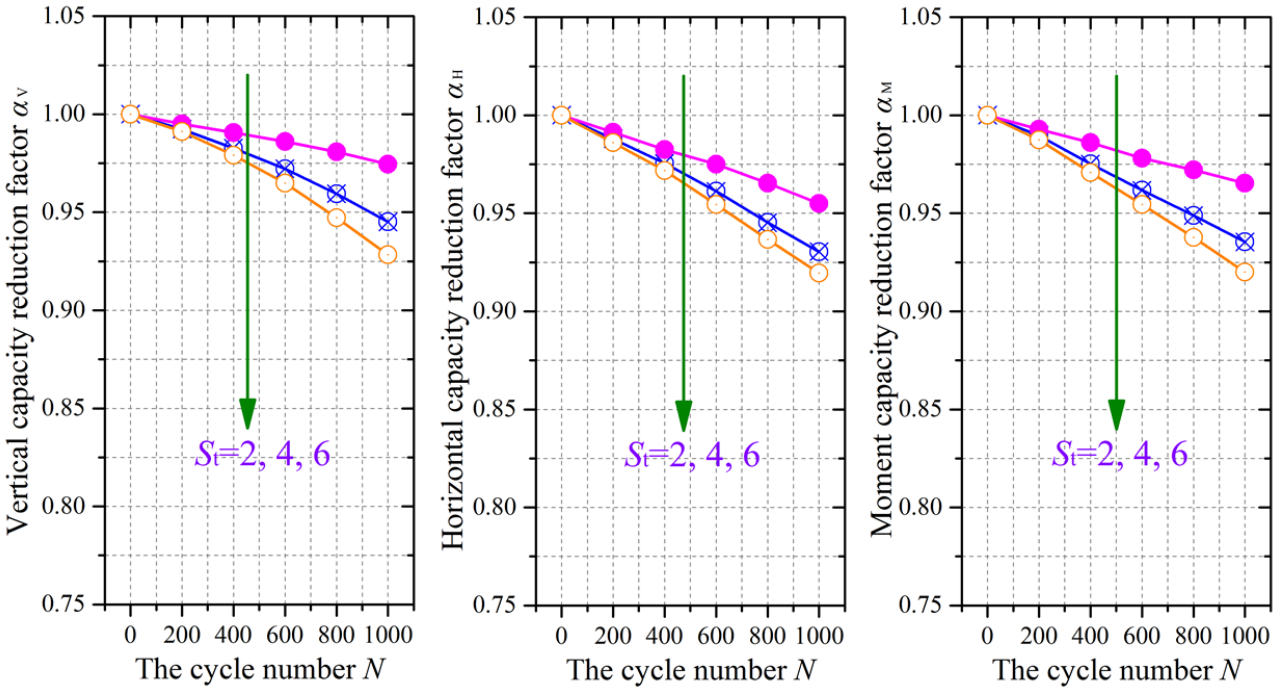

Fig. 14 Effect of soil sensitivity, S_t on post-cyclic capacity

656

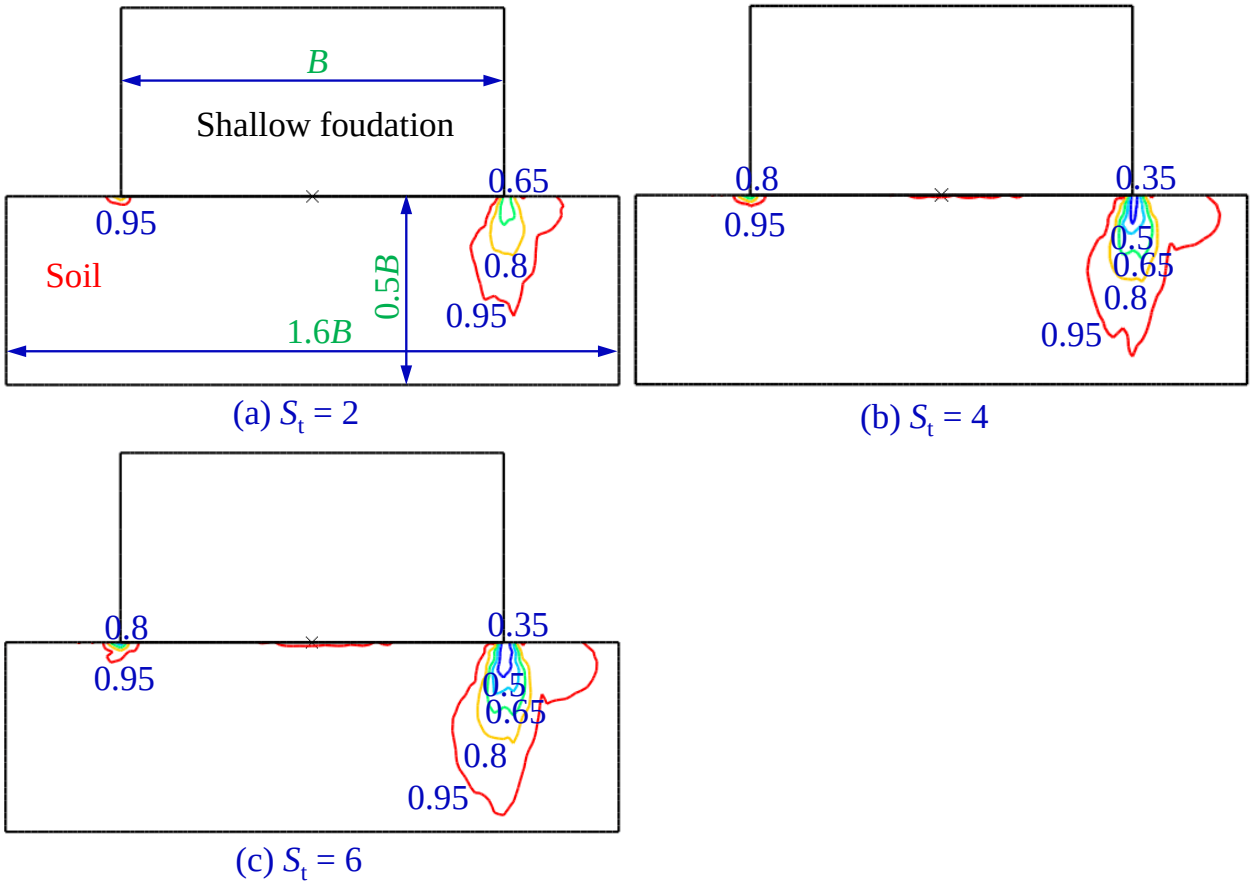

Fig. 15 Effect of soil sensitivity, S_t on degradation factor β_s of shear strength s_u when N=1000

657

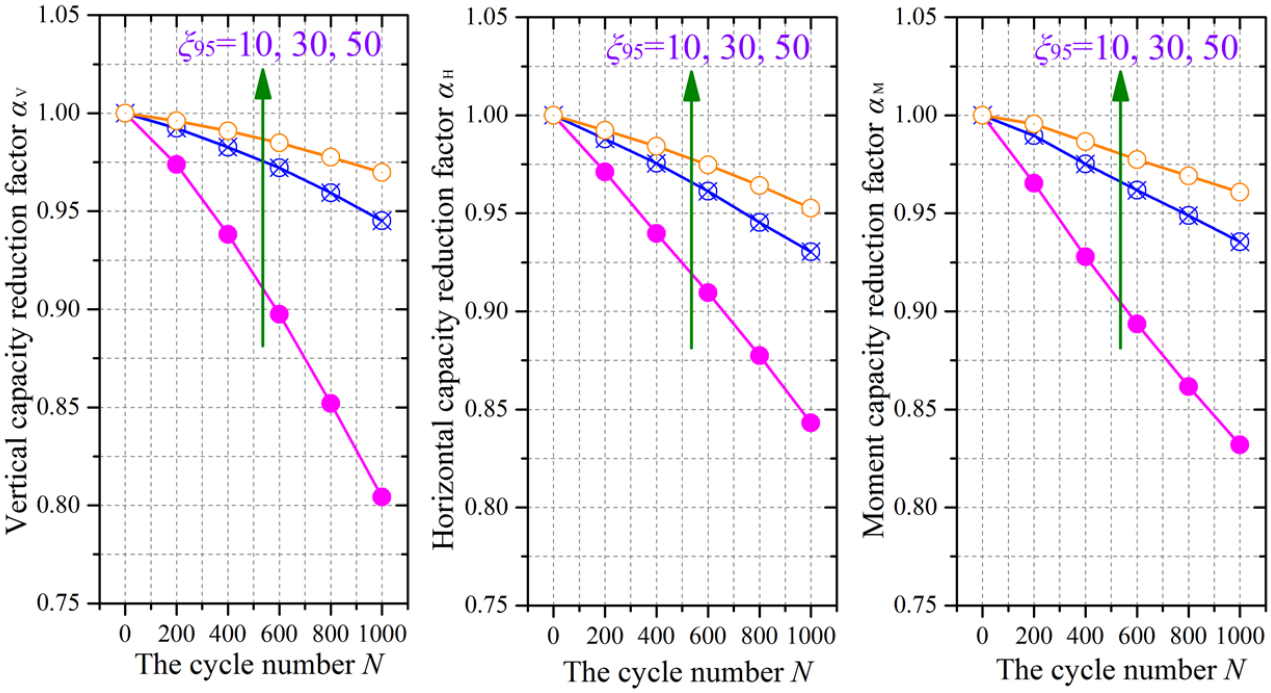

Fig. 16 Effect of soil ductility parameter, ξ_{95} on post-cyclic capacity

658

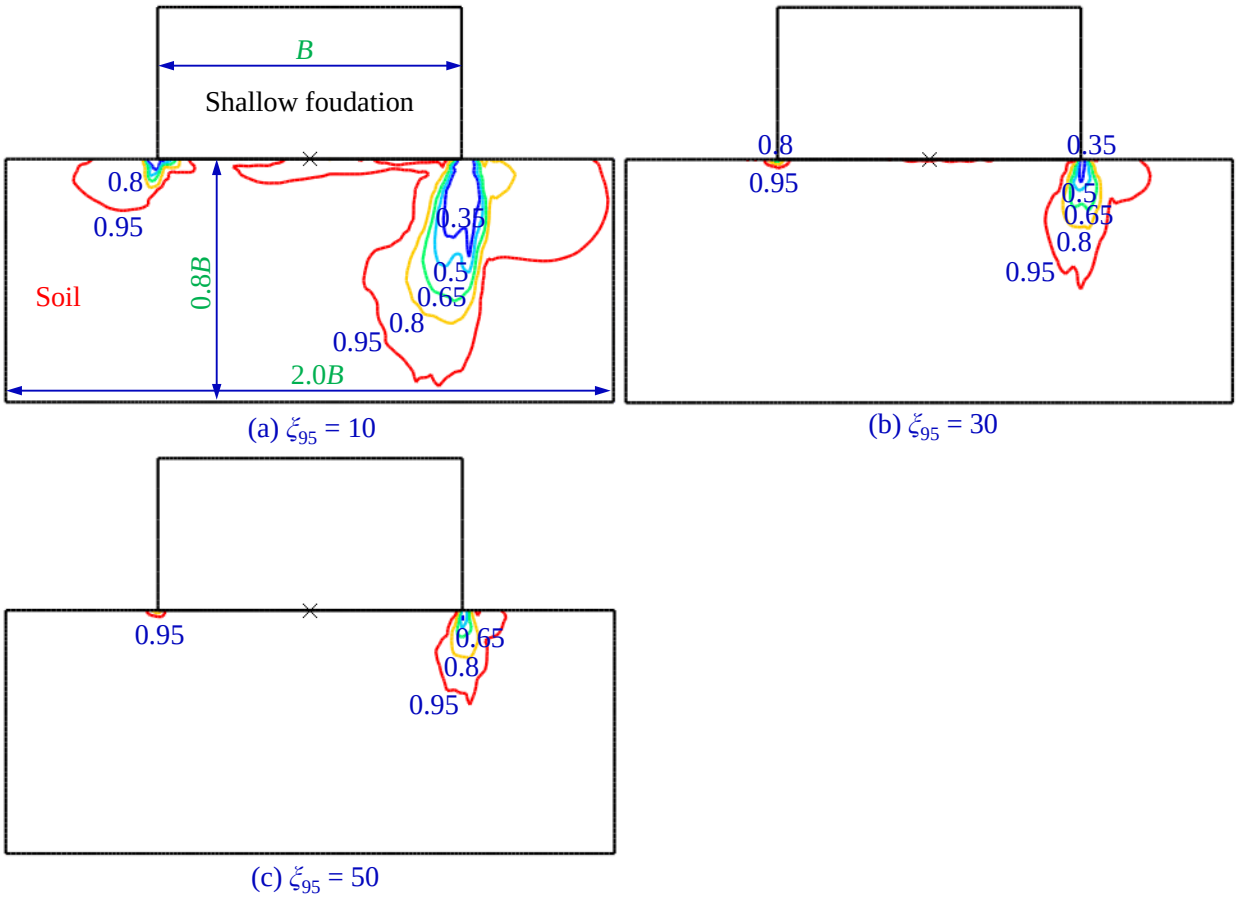

Fig. 17 Effect of soil ductility parameter, ξ_{95} on degradation factor β_s of shear strength s_u when N=1000

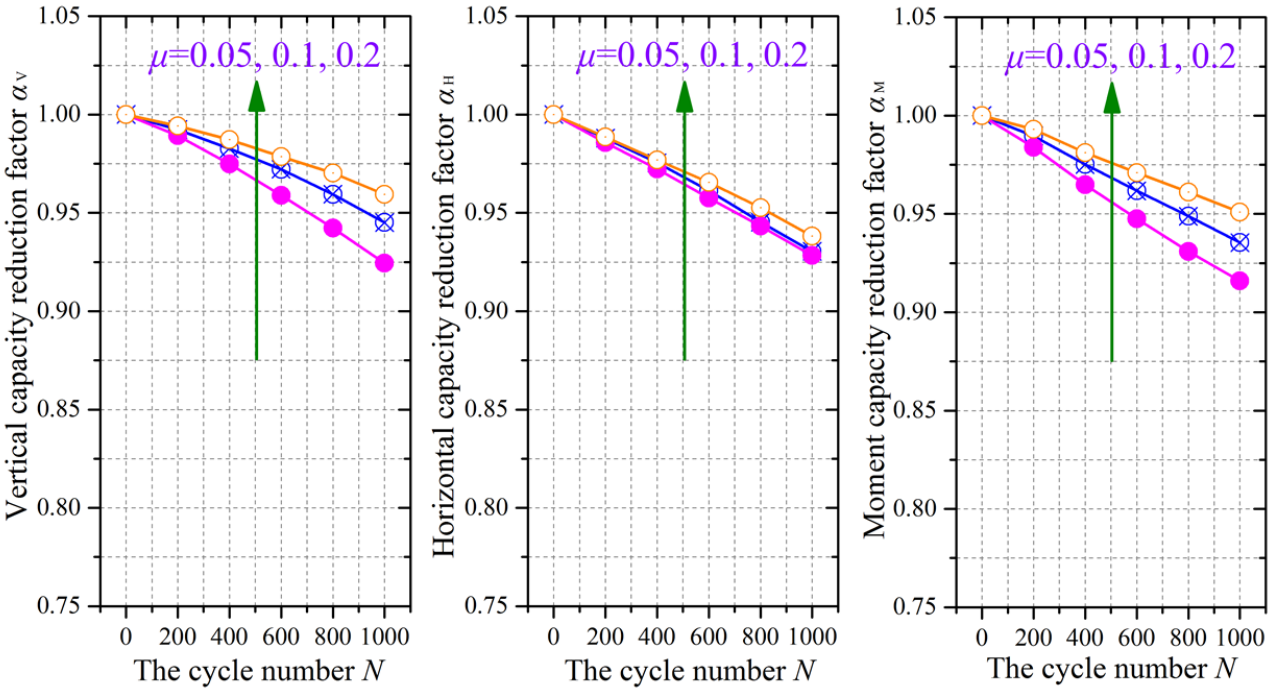

Fig. 18 Effect of soil rate parameter, μ on post-cyclic capacity

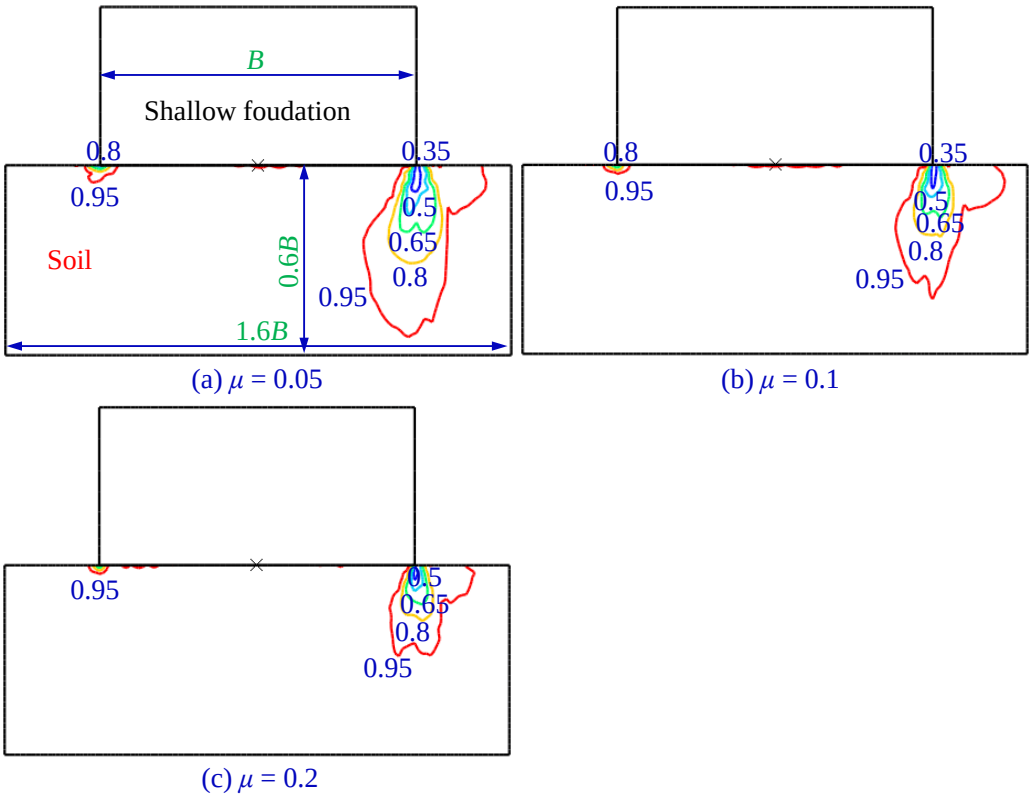

Fig. 19 Effect of soil rate parameter, μ on degradation factor β_s of shear strength s_u when N=1000

661

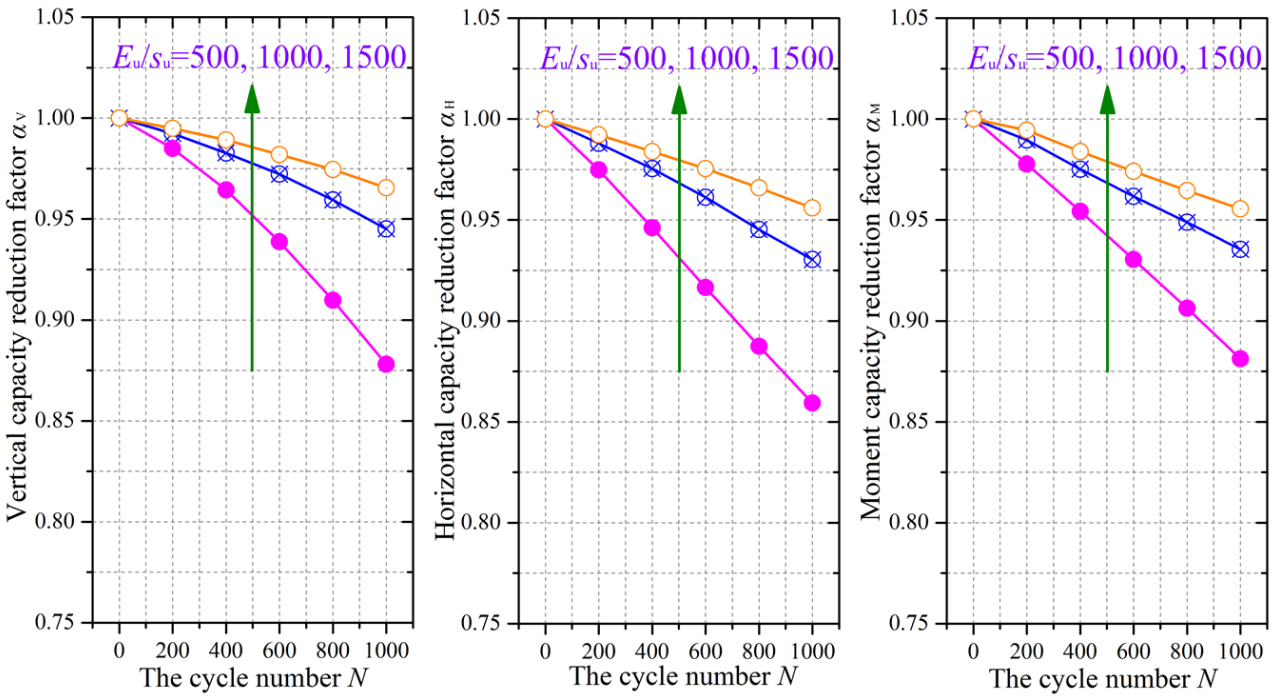

Fig. 20 Effect of stiffness index, E/S_u on post-cyclic capacity

662

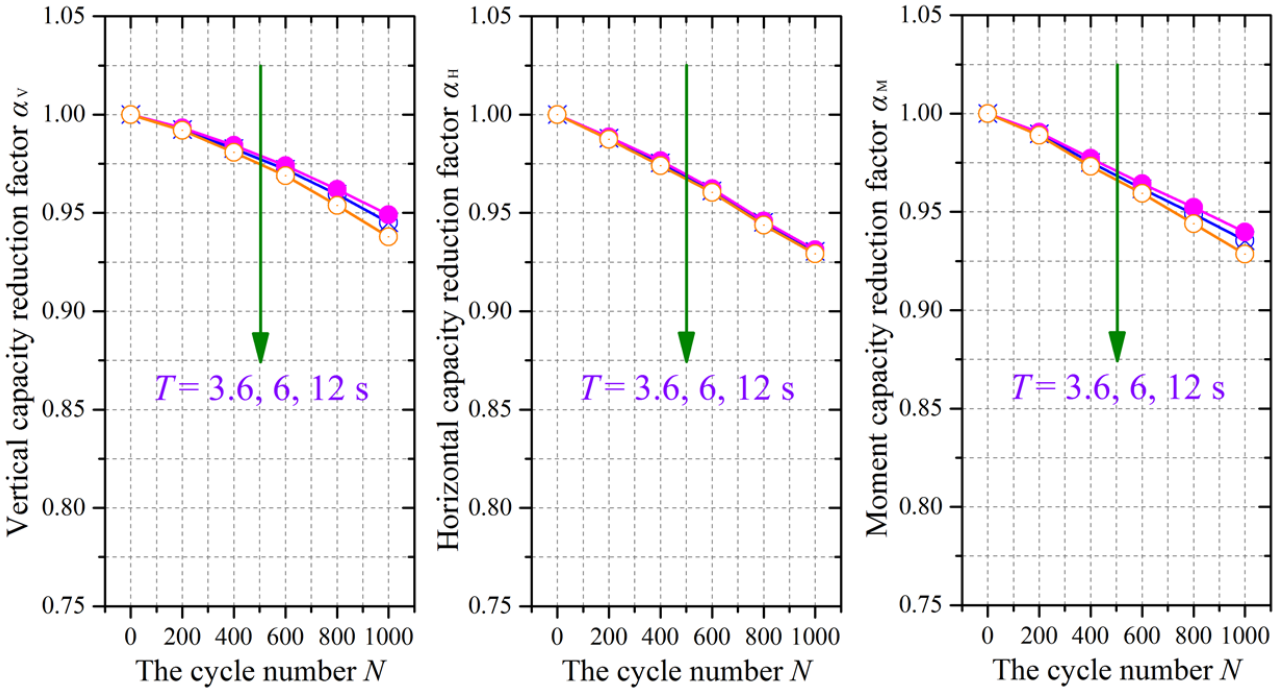

Fig. 21 Effect of period of cyclic loading, T on post-cyclic capacity

663